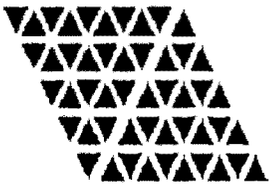

A COMPUTATIONAL COURSE ON

Combined Finite/Discrete Element Method

S. Mohammadi

Department of Civil Engineering
University of Tehran
Tehran, IRAN
http://web.ut.ac.ir/eng/cie/mohammadi

December 2005

Contents

1 Introduction **1**

1.1 Discontinuum Mechanics, Why ? 1

1.2 Discontinuum Mechanics, A Review 3

1.2.1 Rock Blasting 4

1.2.2 Shear Band Slope Stability 4

1.2.3 Granular Flow in Silos 5

1.2.4 Penetration of a Missile 6

1.2.5 Masonry Structures 6

2 Constraint Enforcing Methods **11**

2.1 Introduction 11

2.2 Definition of a Constraint 11

2.2.1 An Example 12

2.3 Constraint Enforcement 13

2.3.1 Penalty Method 14

2.3.2 An example 18

2.4 Contact Instability 20

2.5 Equilibrium Equation 21

2.6 Energy Balance 23

3 Discontinuum Contact Mechanics **27**

3.1 Introduction 27

3.1.1 Historical Development 28
3.2 Contact Detection 28
3.2.1 Contact Geometry 30
3.2.2 Global Search Algorithms 31
3.2.3 Binary Tree Structures 31
3.3 Object Representation 33
3.3.1 Circular Disks 34
3.3.2 Ellipse Shaped Particles 42
3.3.3 Superquadric Objects 44

Chapter 1

Introduction

1.1 Discontinuum Mechanics, Why ?

An interesting set of problems which have recently attracted special attention, includes the general behaviour of granular materials. In this class of problems, large number of interacting bodies , usually simple rigid elements , are interacting in a domain which will govern the general response of the medium through these individual interactions. The best example, may be the filling or emptying a silo with/from granular materials as depicted in Figure 1.1 [1].

This lack of success was not only limited to that simple case; almost anywhere in the industry and academic world, several applications could have been found that analysts ceased to be able to accurately simulate. One of the major deficiencies was in the field of new advanced materials being subjected to dynamic and hazardous loadings.

Figure 1.2 represents the progressive fracturing and fragmentation phenomena in a typical composite specimen subjected to impact loading. This schematic representation, is perhaps only related to the failure observed in high velocity impact. For low velocity impact, however, while it is unlikely that extensive fragmentation will be observed, material fracture and delamination will be the likely modes of failure that exist.

The traditional approach to the simulation of stress distributions in arbitrary shaped components under possible nonlinear geometric and material conditions is by finite element techniques. However, the traditional finite element method (FEM) is rooted in the concepts of continuum mechanics and is not suited to general fracture propagation problems since it necessitates that discontinuities be propagated along the predefined element boundaries. The corresponding elasticity and fracture mechanics concepts are applicable only in situations dealing with a single crack or a low-fractured area without any fragmentation [2]. In contrast, the *discrete element method* (DEM) is specifically designed to solve problems that exhibit strong discontinuities in material and geometric behaviour [3]. The discrete element method idealizes the whole medium into an assemblage of individual bodies, which in addition to their own deformable response, interact with each other (through a contact type interaction) to perform the same response as the medium [4]. A far more natural and general approach is offered by a combination of discrete element and finite element methods.

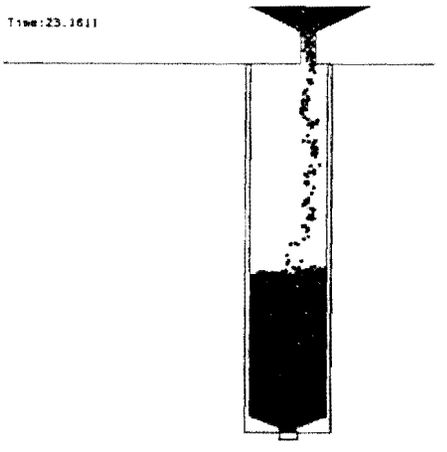

Figure 1.1: Filling a silo with granular material [1].

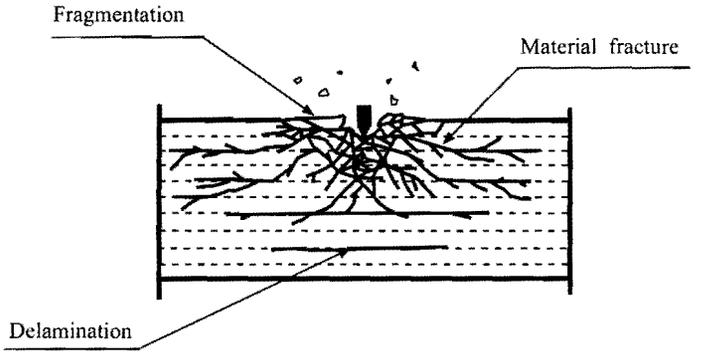

Figure 1.2: Progressive fracturing and fragmentation in a typical composite specimen subjected to impact loading.

1.2 Discontinuum Mechanics , A Review

To attain a realistic overview of the extent a contact based algorithm can be used for analysing various academic, engineering and industrial problems, a quick review of potential applications are provided. It is not intended, primarily, to compare the results with available data in the literature, as it is usual in academic papers, but to illustrate to the reader the applicability of the method to different applications that may be analysed by the use of the computational discontinuum mechanics. It is also aimed at sparking new ideas for further research and future challenges in this subject.

This chapter reviews the following engineering applications, amongst many others, which are currently being researched in many of research institutions throughout the world,

- Geomechanical applications
- Granular materials
- Impact analysis (progressive fracturing)
- Particulate flow
- Computer graphics

1.2.1 Rock Blasting

Rock blasting is an interesting area for application of discrete element method. Results shown in this section are taken from [5], based on using a simplified solid rock - detonation gas interaction models.

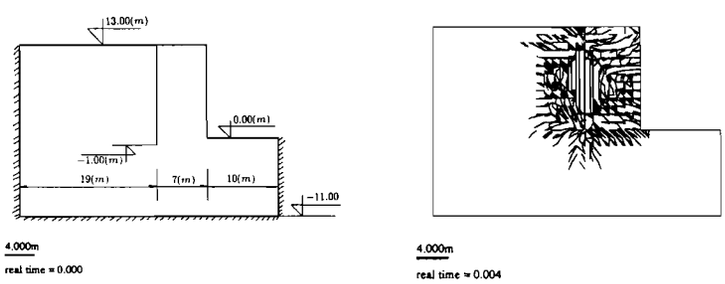

Figure 1.3: A 2D bench blasting simulation [5].

1.2.2 Shear Band Slope Stability

In contrast to the DDA method, a shear band slope stability analysis may be performed by using a fully deformable nonlinear finite element simulation. An adaptive remeshing scheme has to be employed to avoid excess distortions of the finite elements close to the highly deformed shearing band.

The concept of shear band deformation can be best understood from Figure 1.4 which depicts the deformation process of a simple plate with an initial circular hole subjected to a set of tensile forces [6].

Figure 1.5 illustrates two different examples of slope instability simulations performed by Stead et. al. [7] and Cramer et. al. [8] in two and three dimensions, respectively. In the 2D case, an h-adaptive finite element method has been adopted, whereas in the 3D example, only large deformation theory has been considered.

1.2.3 Granular Flow in Silos

Silos represent a vital part of the industrial infrastructure. Failure of a silo often causes great economic losses either by wasting the ensiled materials, delaying production lines or disrupting transportation plans. In this example, the prediction of pressure and flow in silos has been investigated utilizing the discrete element method. (Silo and granular material are both modelled in this approach) [9, 10]. The results of typical conducted analyses may be used to guide the silo design procedures by pointing out any unanticipated loading conditions and pressure distributions which might arise during operation, as well as phenomena such as arching, different filling/emptying regimes, seismic loading, etc..

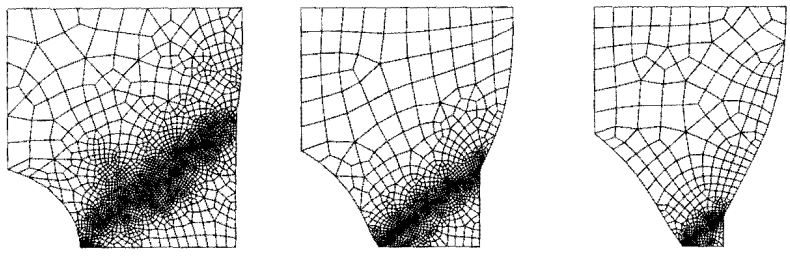

Figure 1.4: Remeshing process and the 45° shear band development in a tensile plate undergoing large lateral necking phenomenon.

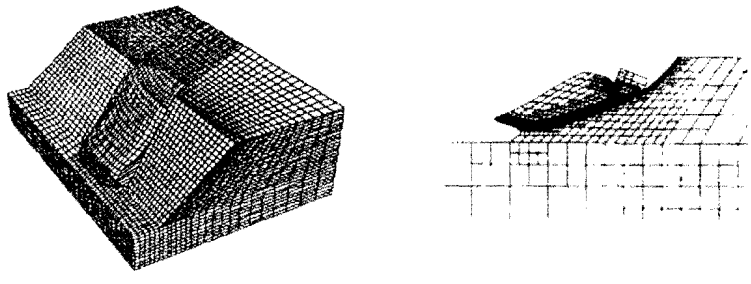

Figure 1.5: Two shear band slope instability problems [7, 8].

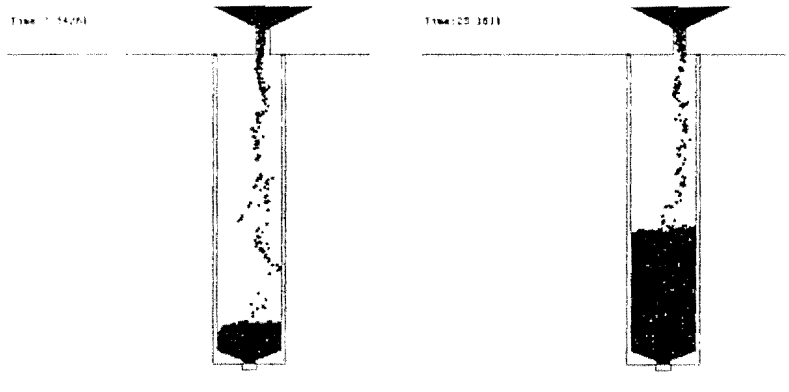

Figure 1.6: Discrete element modelling of granular flow in a typical silo [9].

1.2.4 Penetration of a Missile

Structural design of a shelter, armored military equipment and safety measures for bullet-proof vests may force a designer/analyst to check for impenetrability response of a structure subjected to a high velocity object. A complete analysis of an object penetrating a structure and developing extensive damage in it, has only become possible by the use of combined finite/discrete element techniques.

Figure 1.7, illustrates how the crack patterns are propagated within a typical ceramic plate as a bullet penetrates the plate in different time steps.

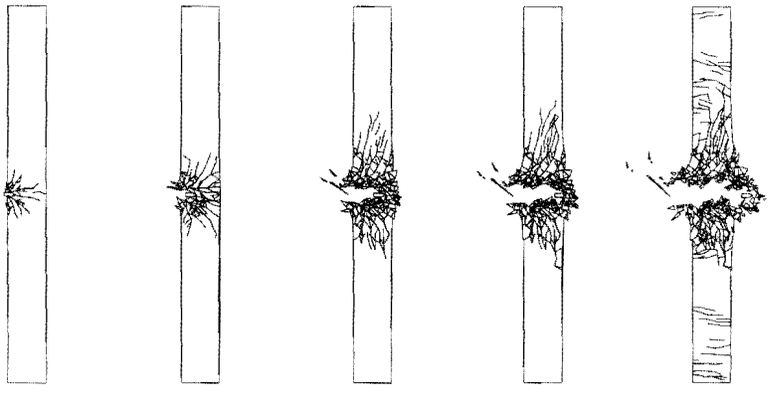

Figure 1.7: Progressive fracturing in a structure impacted by a high velocity bullet.

1.2.5 Masonry Structures

Several interesting implementations of the discrete element method have been proposed for predicting the bahaviour of masonry structures [1, 11, 12, 13]. Nevertheless, the predictive modelling of the non-linear behaviour of masonry structures remains a challenge, due to their semi-discrete and composite nature.

As a real simulation, Figure 1.8 shows a 50 years old railroad two span masonry bridge and the finite/discrete element model. The bridge was incrementally loaded in place until severe cracking and large bridge key deformation were observed as reported by Marefat et. al. [14].

A combined finite/discrete element simulation was performed to simulate the failure behaviour of the structure. Cracking patterns similar to the test observations were predicted according to Figure 1.9 [15].

Another example; the Strathmashie Bridge, 150 years old, was of rubble masonry, in reasonable condition and showing little distortion, but there seemed to be very little mortar in parts of the arch.

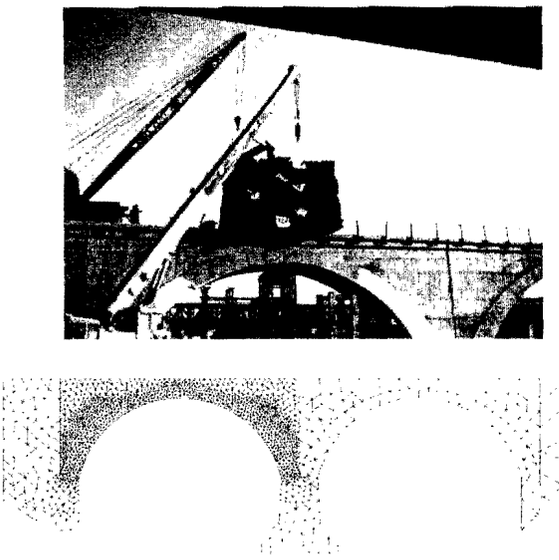

Figure 1.8: A two span masonry bridge and the finite element model [14].

An experimental test was performed to assess the performance of the masonry bridge until the collapse of the structure, Figure 1.10. A numerical simulation was performed by Klerck [13] based on a combined finite/discrete element technique, as depicted in Figure 1.11. The failure modes are interestingly similar to one observed in experimental test [16].

Figure 1.9: Crack propagation patterns at different times [14].

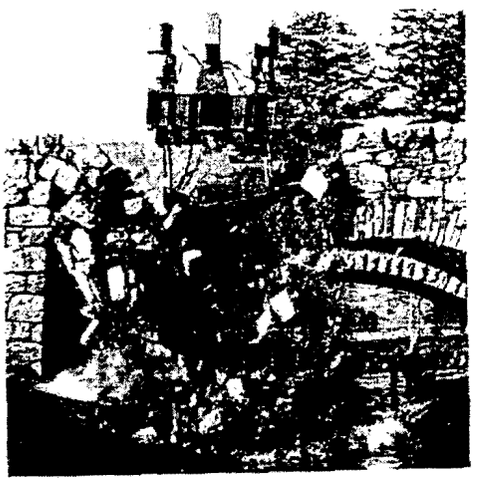

Figure 1.10: An experimental collapse test for a masonry bridge.

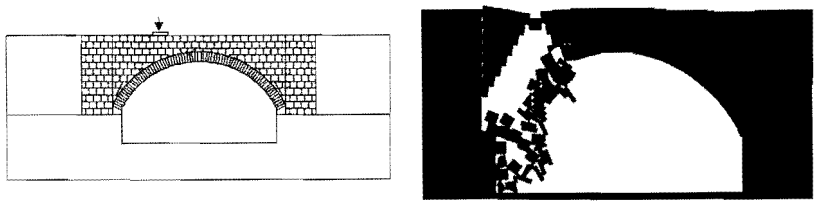

Figure 1.11: Finite element simulation of the collapsing bridge [13].

Chapter 2

Constraint Enforcing Methods

2.1 Introduction

Many different methods have been developed for enforcing a constraint condition on the governing equation of a well established physical behaviour. In this chapter, the following four methods for enforcement of constraints within a finite element analysis are reviewed:

- Penalty method
- Lagrange multiplier method
- Perturbed Lagrangian method
- Augmented Lagrangian method

Here only the penalty method is described in detail.

2.2 Definition of a Constraint

A constraint either prescribes a value for a freedom (single point constraint) or a relationship between two or more freedoms (multipoint constraint). Figure 2.1 represents a typical *impenetrability* constraint between two contacting bodies. This constraint defines the necessary conditions to prevent the bodies from penetrating each other.

The mathematical description of a constraint equation may be written in the form

$$\boldsymbol{C}\boldsymbol{u} = \boldsymbol{Q} \tag{2.1}$$

where $\boldsymbol{C}$ is a matrix of constraints, $\boldsymbol{u}$ is the vector of freedom and $\boldsymbol{Q}$ is a vector of constants. $\boldsymbol{Q}$ in many cases may become a null vector.

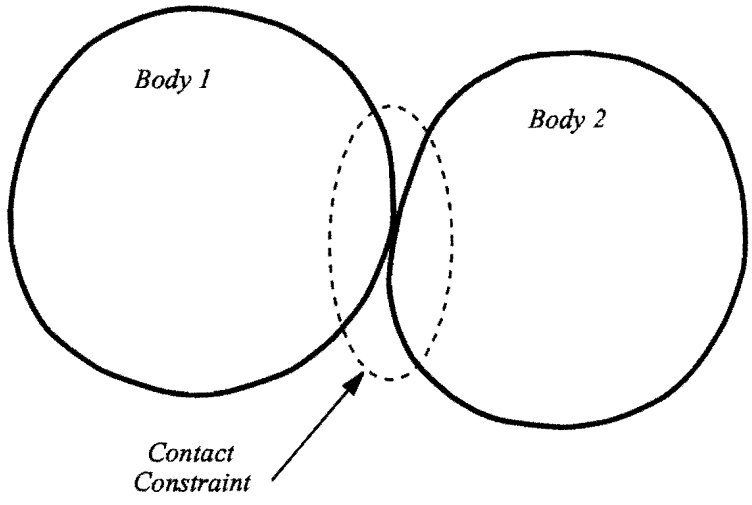

Figure 2.1: Impenetrability constraint for two contacting bodies.

2.2.1 An Example

Two straight bars which are just in contact are depicted in Figure 2.2. Each node has a single degree of freedom along the bar direction. A 0.1 unidirectional rightward displacement is applied to node 1 of the left bar.

Each bar behaves as a linear spring, so

$$K_1 = K_2 = \begin{bmatrix} 10 & -10 \\ -10 & 10 \end{bmatrix} \tag{2.2}$$

The assembled system of equations will be

$$\begin{bmatrix} 10 & -10 & 0 & 0 \\ -10 & 10 & 0 & 0 \\ 0 & 0 & 10 & -10 \\ 0 & 0 & -10 & 10 \end{bmatrix} \begin{bmatrix} u_1 = 0.1 \\ u_2 \\ u_3 \\ u_4 = 0 \end{bmatrix} = \begin{bmatrix} f_1 \\ 0 \\ 0 \\ f_4 \end{bmatrix} \tag{2.3}$$

since the equations are uncoupled, the results will be:

$$\begin{cases} u_2 = 0.1 \\ u_3 = 0 \end{cases} \tag{2.4}$$

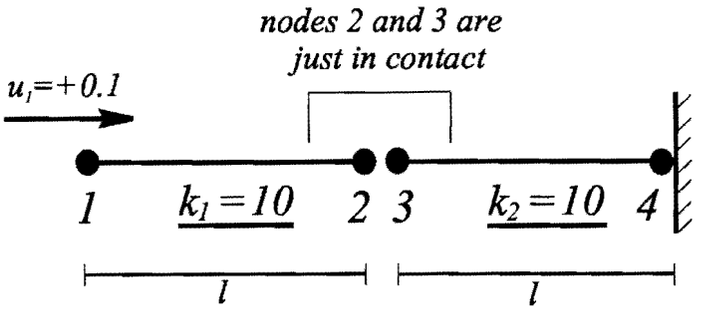

Figure 2.2: A simple two bar model.

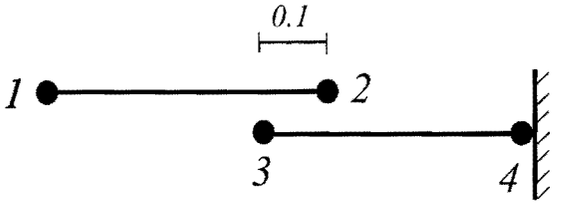

Figure 2.3: Uncoupled solution for the two bar problem.

Figure 2.3 shows the deformed shapes of the bars for this analysis, which clearly shows overlapping the elements.

To avoid this, the following constraint equation should be enforced:

$$u_3 - u_2 \geq 0 \tag{2.5}$$

We will later use this simple example to verify the methods adopted as constraint enforcing methods.

2.3 Constraint Enforcement

Equation (2.1) should be added to the conventional equations of the system and solved simultaneously. Different approaches have been proposed for solving this set of equations which will be briefly reviewed

and compared.

One approach, which has been widely used by many researchers, is the concept of minimization of the total potential energy for deriving the necessary equations. The total potential energy of a linear elastic system subjected to static loading and consisting of two discrete bodies, Ω_1 and Ω_2 may be written as (Figure 2.4)

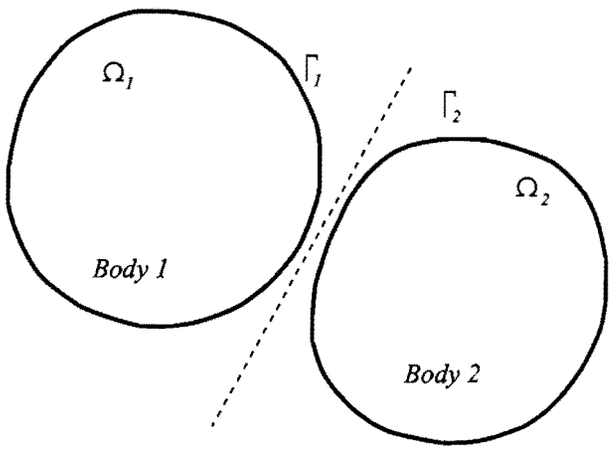

Figure 2.4: A system consisted of two interacting bodies.

$$\Pi = \int_{\Omega_1+\Omega_2} \frac{\partial u_i}{\partial x_j} \sigma_{ij} d\Omega - \int_{\Omega_1+\Omega_2} u_i b_i d\Omega - \int_{\Gamma_1+\Gamma_2} u_i t_i d\Gamma \tag{2.6}$$

Using a standard discretization procedure based on appropriate trial functions

$$\Pi(\boldsymbol{u}) = \frac{1}{2}\boldsymbol{u}^T \boldsymbol{K}\boldsymbol{u} - \boldsymbol{u}^T \boldsymbol{R} \tag{2.7}$$

where $\boldsymbol{u}$ is the nodal displacement vector, $\boldsymbol{K}$ is the system stiffness matrix and $\boldsymbol{R}$ is the force vector. Without additional constraint equation, bodies Ω_1 and Ω_2 do not interact and the system is uncoupled.

2.3.1 Penalty Method

The Penalty method was probably the first approach adopted for a constraint enforcing method. It was developed by Hallquist and his colleagues in Lawrence Livermore National Laboratory during the

late seventies for modelling impact/contact problems.

To obtain the necessary equations, and comparing to the first term in Equation (2.7), the total potential energy for a constrained problem can be written as

$$\bar{\Pi}(\boldsymbol{u}) = \Pi(\boldsymbol{u}) + \frac{1}{2}\boldsymbol{g}^T\alpha\boldsymbol{g} \tag{2.8}$$

where α is a normal contact stiffness, called penalty number, and in general is a diagonal matrix of penalty terms for each degree of freedom. $\boldsymbol{g}$ is the normal gap vector and for $\boldsymbol{g} = \boldsymbol{0}$ the constraints are fully satisfied; $\bar{\Pi}(\boldsymbol{u}) = \Pi(\boldsymbol{u})$.

Minimization of the total potential energy will result to

$$\delta\bar{\Pi} = \left[\frac{\partial\Pi}{\partial\boldsymbol{u}}\delta\boldsymbol{u} + \boldsymbol{g}^T\alpha\frac{\partial\boldsymbol{g}}{\partial\boldsymbol{u}}\delta\boldsymbol{u}\right] \tag{2.9}$$

$$\delta\bar{\Pi} = \left[\frac{\partial\Pi}{\partial\boldsymbol{u}} + \boldsymbol{g}^T\alpha\frac{\partial\boldsymbol{g}}{\partial\boldsymbol{u}}\right]\delta\boldsymbol{u} \tag{2.10}$$

To maintain equilibrium, $\delta\bar{\Pi}$ should be equal to 0.

The first term on the right hand side of (2.10) is the well known stiffness equation

$$\frac{\partial\Pi}{\partial\boldsymbol{u}} = \boldsymbol{K}\boldsymbol{u} - \boldsymbol{R} \tag{2.11}$$

and for the second term, we have

$$\boldsymbol{g} = \boldsymbol{C}\boldsymbol{u} - \boldsymbol{Q} \tag{2.12}$$

$$\frac{\partial\boldsymbol{g}}{\partial\boldsymbol{u}} = \boldsymbol{C} \tag{2.13}$$

$$\boldsymbol{g}^T\alpha\frac{\partial\boldsymbol{g}}{\partial\boldsymbol{u}} = (\boldsymbol{C}\boldsymbol{u} - \boldsymbol{Q})^T\alpha\boldsymbol{C} = \boldsymbol{C}^T\alpha\boldsymbol{C}\boldsymbol{u} - \boldsymbol{C}^T\alpha\boldsymbol{Q} \tag{2.14}$$

Therefore, the modified stiffness equation will be

$$\left[\boldsymbol{K} + \boldsymbol{C}^T\alpha\boldsymbol{C}\right]\boldsymbol{u} = \boldsymbol{R} + \boldsymbol{C}^T\alpha\boldsymbol{Q} \tag{2.15}$$

The term, $\boldsymbol{C}^T\alpha\boldsymbol{C}$ should be added to the system stiffness matrix to incorporate the impenetrability constraint stiffness.

The main features of this method are:

- Enforcement of constraints requires no extra equations.
- The constraints are only satisfied in an approximate manner and the correct range of penalty numbers have to be chosen. If α is too low, the constraints are poorly satisfied, while if α is too large, the stiffness matrix becomes poorly conditioned (the difference between in and out of diagonal terms becomes very high). As an initial estimate for α

$$0.5E < \alpha < 2.0E \tag{2.16}$$

  where E is the young modulus of the contacting bodies.
- For explicit dynamic applications, large values of α may result in a reduction in the critical time step. Large penalty values simulate stiff constraint spring, increasing the global stiffness and so reducing the required critical time step.
- $\alpha \boldsymbol{g}$ corresponds to the penalty force required to enforce the constraint.

The development and implementation of the penalty method for contact applications may be attributed to the work by Hallquist [17] in the late seventies.

The general aspects of the penalty method for imposing a constraint equation has been discussed in the previous section. Here, further details of the scheme as a contact interaction algorithm are discussed. In a contact mechanics analysis, the constraint condition is the impenetrability of the contacting objects. The impenetrability constraint equation for two nodes in direct contact may be expressed from equation (2.1)

$$\boldsymbol{C} \equiv \boldsymbol{u}_2 - \boldsymbol{u}_1 = \boldsymbol{0} \tag{2.17}$$

In some applications, the exact impenetrability is strictly sought. For instance, in simulations of molecular dynamics or animations. These cases usually comprise sparse populations of bodies moving around at high speed and interact by collision. The collisions are brief and can be modelled as instantaneous exchanges of momentum, in which energy may or may not be conserved by the particle pair [18].

In a penalty method, penetration of the contactor object is used to establish the contact forces between contacting objects at any given time (See Figure 2.5).

The general form of equation (2.17) for contact between two bodies may then be defined by [19, 20]

$$\mathbf{g} = [\boldsymbol{x}^2 - \boldsymbol{x}^1] \cdot \boldsymbol{n} \geq 0 \qquad \text{on } \Gamma_c \tag{2.18}$$

where $\mathbf{g}$ is the gap function, $\boldsymbol{x}^1$ and $\boldsymbol{x}^2$ are the deformed configuration of body 1 and 2, respectively, $\boldsymbol{n}$ is the normal to the body at the contact surface, and Γ_c is the contact domain, $\Gamma_c = \Gamma^1 \cap \Gamma^2$.

Therefore, the variational form of the constraint equation (??) may be explicitly expressed as

$$\delta \mathcal{W}^{con} = \int_{\Gamma_c} \alpha \, \mathbf{g} \, \delta \mathbf{g}(\boldsymbol{u}) \, da \tag{2.19}$$

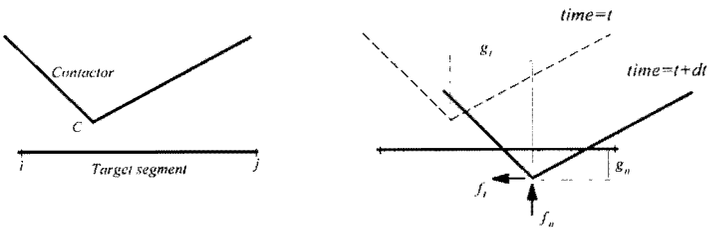

a) Before contact *b) Possible normal and tangential gaps*

Figure 2.5: Contact force based on impenetrability.

$$\delta \mathcal{W}^{con} = \int_{\Gamma_c} \alpha \, \mathbf{g} \, \frac{\partial \mathbf{g}}{\partial \boldsymbol{u}} \, \delta \boldsymbol{u} \, da \tag{2.20}$$

Equation (2.20) may be re-written in terms of the contact force vector

$$\delta \mathcal{W}^{con} = \int_{\Gamma_c} \boldsymbol{f}^{con} \, \frac{\partial \mathbf{g}}{\partial \boldsymbol{u}} \, \delta \boldsymbol{u} \, da \tag{2.21}$$

Attention is now focused on a single boundary node in contact to formulate the residual contribution of contact constraint, $\mathbf{r}^c$. The component form of the virtual work of the contact forces associated to the contact node is then given by [21]:

$$\delta \mathcal{W}^{\text{con}} = f_k^{con} \, \delta \mathrm{g}_k = f_k^{con} \, \frac{\partial \mathrm{g}_k}{\partial u_i^s} \, \delta u_i^s \tag{2.22}$$

where $k = n, t$ and $i = x, y$, and u_i^s is the the i-component of displacement vector at node s, $\mathbf{g} = (\mathrm{g}_n, \mathrm{g}_t)$ is the relative motion (gap) vector in normal and tangential directions, respectively, and $\boldsymbol{f}^{con}$ is the contact force vector over the contact area A^c,

$$\boldsymbol{f}^{con} = A^c \, \boldsymbol{\sigma}^c \quad , \quad \boldsymbol{\sigma}^c = \boldsymbol{\alpha} \, \mathbf{g} = \begin{bmatrix} \alpha_n & 0 \\ 0 & \alpha_t \end{bmatrix} \begin{bmatrix} \mathrm{g}_n \\ \mathrm{g}_t \end{bmatrix} \tag{2.23}$$

where $\boldsymbol{\alpha}$ is the penalty term matrix, which can vary for normal and tangential gaps and even between single contact nodes. The corresponding recovered residual force is then evaluated as:

$$r_i^s = f_k^{con} \, \frac{\partial \mathrm{g}_k}{\partial u_i^s} \tag{2.24}$$

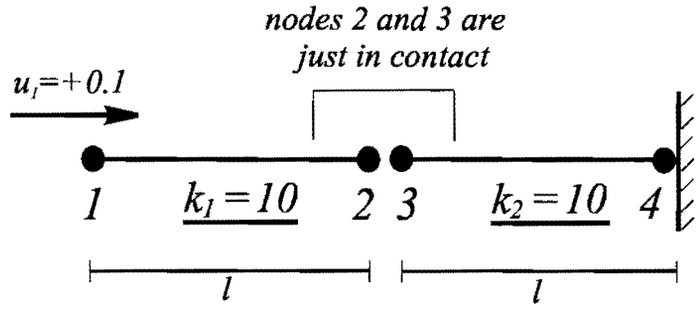

Figure 2.6: A simple two bar model.

The partial derivative part of equation (2.24) defines the direction and distribution of normal and tangential contact forces. The calculated contact force has then to be distributed to the target and contactor nodes.

2.3.2 An example

To illustrate how to use the penalty method for enforcing a constraint equation, Example 3 of Section 2.2.1 is re-considered (Figure 2.6).

The constraint equation may be written as

$$u_3 - u_2 \geq 0 \tag{2.25}$$

with

$$\boldsymbol{C} = \begin{matrix} u_2 & u_3 \end{matrix} \begin{bmatrix} -1 & +1 \end{bmatrix} \tag{2.26}$$

for a constant value of α

$$\alpha \boldsymbol{C}^T \boldsymbol{C} = \alpha \begin{bmatrix} 1 & -1 \\ -1 & 1 \end{bmatrix} \tag{2.27}$$

which is similar to the stiffness of a spring attached to the bars.

The assembled system of equations will then be

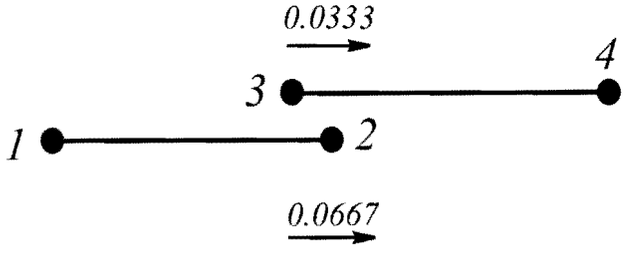

Figure 2.7: Remaining penetration in a two bar contact problem using the penalty method.

$$\begin{bmatrix} 10 & -10 & 0 & 0 \\ -10 & 10+\alpha & -\alpha & 0 \\ 0 & -\alpha & 10+\alpha & -10 \\ 0 & 0 & -10 & 10 \end{bmatrix} \begin{bmatrix} u_1 = 0.1 \\ u_2 \\ u_3 \\ u_4 = 0 \end{bmatrix} = \begin{bmatrix} f_1 \\ 0 \\ 0 \\ f_4 \end{bmatrix} \tag{2.28}$$

Equation (2.28) is a coupled equation due to the existence of non-diagonal α terms.

To continue the solution procedure only consider the active part

$$\begin{bmatrix} 10+\alpha & -\alpha \\ -\alpha & 10+\alpha \end{bmatrix} \begin{bmatrix} u_2 \\ u_3 \end{bmatrix} = \begin{bmatrix} 1 \\ 0 \end{bmatrix} \tag{2.29}$$

solving for unknown u_2 and u_3

$$\begin{bmatrix} u_2 \\ u_3 \end{bmatrix} = \frac{1}{(10+\alpha)^2 - \alpha^2} \begin{bmatrix} 10+\alpha & \alpha \\ \alpha & 10+\alpha \end{bmatrix} \begin{bmatrix} 1 \\ 0 \end{bmatrix} \tag{2.30}$$

To get some numbers, for $\alpha = 10$

$$\begin{bmatrix} u_2 \\ u_3 \end{bmatrix} = \frac{1}{300} \begin{bmatrix} 20 & 10 \\ 10 & 20 \end{bmatrix} \begin{bmatrix} 1 \\ 0 \end{bmatrix} = \begin{bmatrix} 0.0667 \\ 0.0333 \end{bmatrix} \tag{2.31}$$

the results show the existence of some penetration of bar 1 into the bar 2 (See Figure 2.7).

Table 2.1 summarizes the results obtained for the same equation using different penalty numbers. It is clearly seen that by increasing the penalty number the solution converges to the exact solution.

α	u_2	u_3
10	.0667	.0333
100	.0523	.0476
1000	.0502	.0497
10000	.0500	.0500

Table 2.1: Results for different penalty numbers.

2.4 Contact Instability

One of the concerns of using the penalty method as a numerical constraint scheme for explicit analysis is its stability. The reason can be attributed to the fact that the impenetrability condition ($g = 0$) is only approximately satisfied by this method. This is clearly observed from Equation (2.8) where a non-zero term is added to the total potential energy of the system. Without any additional treatment, the penalty method will cause the system to gain energy artificially, although sometimes this extra energy is a compensation for the loss of deformation energy due to contact penetration.

In a central difference one dimensional contact analysis based on the penalty method, the contact force may be defined as

$$f^{con} = \begin{cases} \alpha g & if\ g > 0 \\ 0 & otherwise \end{cases} \tag{2.32}$$

where g is the normal penetration. One may expect the central difference scheme to be stable when applied with

$$K = \frac{k}{m}\Delta t^2 < 4 \tag{2.33}$$

However, numerical tests show that in some cases considerable energy is added to the system because the central difference scheme becomes unstable [22] (For details of the central difference method see Section ??).

To clarify the problem, consider the impact of a material point (ball) on to a rigid wall as depicted in Figure 2.8.

When the material point enters the wall boundaries, it may happen that for some time $\tau < \Delta t$, the scheme generates no contact force to resist penetration. When the material is leaving the wall boundaries, it can happen that for some time $\tau < \Delta t$, the contact force continues to be pushing out the material point from the boundary, although there is no penetration any longer. Consequently, the material point gains some additional energy each time it enters and leaves the wall boundary. It may happen that $\tau = 0$, but in general this is not the case [22].

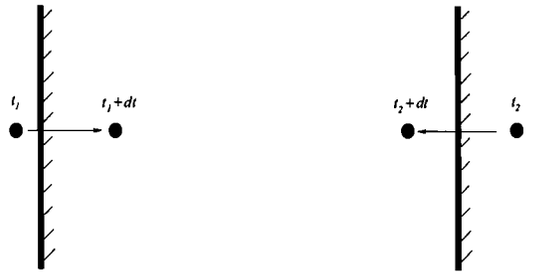

a) The ball penetrating into the wall. *b) The ball escaping out of the wall.*

Figure 2.8: A material point entering and leaving a rigid wall at successive time steps.

2.5 Equilibrium Equation

Consider a body, $\mathcal{B}$, occupying a region Ω with a boundary Γ subject to body forces $\boldsymbol{f}^{body}$ throughout its domain Ω. Here, the boundary is assumed to consist of a part with prescribed displacement u_i, Γ_{u_i}, and a part with prescribed traction force f_i^{surf}, Γ_{σ_i} (Figure 2.9). The boundary conditions may then be described as

$$\begin{array}{lll} \boldsymbol{\sigma n} = \boldsymbol{f}^{\text{surf}} & on & \Gamma_\sigma \\ \boldsymbol{\chi} = \bar{\boldsymbol{\chi}} & on & \Gamma_u \end{array} \tag{2.34}$$

where $\boldsymbol{\sigma}$ represents the Cauchy stress tensor and $\boldsymbol{n}$ represents the unit outer normal along Γ_σ.

For this body to be in a state of static equilibrium, the following condition must be satisfied

$$\int_{\Gamma_\sigma} \boldsymbol{f}^{surf} da + \int_\Omega \boldsymbol{f}^{body} dv = 0 \tag{2.35}$$

and for a state of dynamic equilibrium,

$$\int_{\Gamma_\sigma} \boldsymbol{f}^{surf} da + \int_\Omega \boldsymbol{f}^{body} dv = \int_\Omega \rho \ddot{\boldsymbol{u}} dv \tag{2.36}$$

Applying the divergence theorem to the first term in the above equation and using equation (2.34), the following strong form of equilibrium equation is finally obtained

$$div\boldsymbol{\sigma} + \boldsymbol{f}^{body} = \rho \ddot{\boldsymbol{u}} \tag{2.37}$$

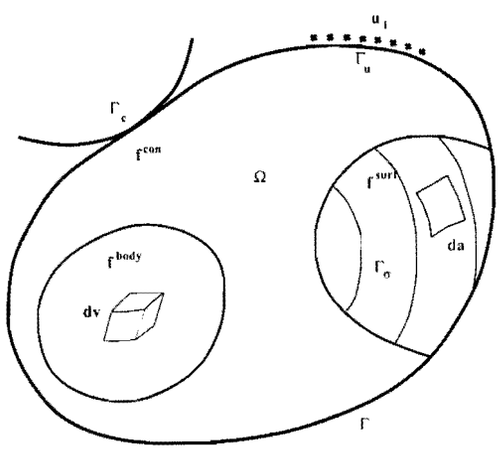

Figure 2.9: Description of the boundary value problem.

which represents the dynamic equilibrium condition at a point within the body.

Here, a weak form of the equilibrium equation is derived, since this is utilized as the basis of the Finite Element procedure:

$$\int_{\Omega} \boldsymbol{\sigma} : \boldsymbol{\nabla} w dv + \int_{\Omega} \rho \ddot{\boldsymbol{u}} w dv = \int_{\Omega} \boldsymbol{f}^{body} w dv + \int_{\Gamma_\sigma} \boldsymbol{f}^{surf} \cdot w da \tag{2.38}$$

According to the Galerkin weighted residual approach for solving the boundary value problem, the weighting functions are chosen as the field of virtual displacements $\delta \boldsymbol{u}$, and the weak form of the equilibrium conditions represented in equation (2.38) is equivalent to the principle of virtual work. More details may be found in Zienkiewicz et al. [23].

In addition, it is assumed that a part of boundary, Γ_c, may be in contact with another body (Figure 2.9) according to the contact boundary conditions [24, 19]

$$\begin{array}{lll} \boldsymbol{\sigma n} = \mathbf{0} & on\ \Gamma_c & if\ \ \mathbf{g}_{\mathrm{N}} > 0 \\ \boldsymbol{\sigma n} = \boldsymbol{f}^{con} & on\ \Gamma_c & if\ \ \mathbf{g}_{\mathrm{N}} \leq 0 \end{array} \tag{2.39}$$

where $\mathbf{g}_{\mathrm{N}}$ is the *gap* between the bodies. By denoting

$$\mathcal{V} := \{\delta \boldsymbol{u} : \delta u_i = 0 \quad \text{on} \quad \Gamma_{u_i}\} \tag{2.40}$$

the space of admissible variations, the variational (weak) form of the dynamic initial/boundary value problem may be expressed as [25, 26]

$$\mathcal{W}^{\text{int}}(\delta\boldsymbol{u},\boldsymbol{u}) + \mathcal{M}(\delta\boldsymbol{u},\boldsymbol{u}) = \mathcal{W}^{\text{ext}}(\delta\boldsymbol{u}) + \mathcal{W}^{\text{con}}(\delta\boldsymbol{u}) \tag{2.41}$$

where

$$\mathcal{W}^{\text{int}}(\delta\boldsymbol{u},\boldsymbol{u}) = \int_{\Omega} \delta\boldsymbol{\epsilon}(\boldsymbol{u}) : \boldsymbol{\sigma}(\boldsymbol{u}) dv \tag{2.42}$$

$$\mathcal{M}(\delta\boldsymbol{u},\boldsymbol{u}) = \int_{\Omega} \delta\boldsymbol{u}\cdot\rho\ddot{\boldsymbol{u}} dv \tag{2.43}$$

$$\mathcal{W}^{\text{ext}}(\delta\boldsymbol{u}) = \int_{\Omega} \delta\boldsymbol{u}\cdot\boldsymbol{f}^{\text{body}} dv + \int_{\Gamma_\sigma} \delta\boldsymbol{u}\cdot\boldsymbol{f}^{\text{surf}} da \tag{2.44}$$

$$\mathcal{W}^{\text{con}}(\delta\boldsymbol{u}) = \int_{\Gamma_c} \delta\mathbf{g}(\boldsymbol{u})\cdot\boldsymbol{f}^{\text{con}} da \tag{2.45}$$

denote, respectively, the virtual work of internal forces, the inertia forces contribution, the virtual work of external forces and the virtual work of contact forces. Here $\boldsymbol{\sigma}$ is the Cauchy stress tensor, $\boldsymbol{\epsilon}$ is the strain tensor, $\boldsymbol{u}$ is the displacement vector, while $\mathbf{g}$ represents the contact gap vector. Observe that in the present formulation the contact terms correspond to a penalty formulation of contact interaction.

2.6 Energy Balance

Numerical instabilities are normally associated with a large growth of energy. Therefore, monitoring the stability and accuracy of the solution can be performed by continuously checking the energy balance of the system. The energy balance equation at time t_n can be expressed as [1],

$$\left|W_n^{ext} - U_n^{kin} - U_n^{str} - W_n^{dam}\right| \leq \delta \left|W_n\right| \tag{2.46}$$

where W_n^{ext} is the work of external forces, U_n^{kin} is the kinetic energy, U_n^{str} is the strain energy, W_n^{dam} is the dissipation energy due to work by damping forces, δ is the specified allowable tolerance of the analysis, and W_n is some norm of energy,

$$\left|W_n\right| = \left|U_n^{kin}\right| + \left|U_n^{str}\right| \tag{2.47}$$

which is suitable for discrete element contact problems. These energy terms may be expressed as,

$$W_n^{ext} = W_n^{surf} + W_n^{body} \tag{2.48}$$

$$W_n^{surf} = \int_\Gamma \left[\int_{\boldsymbol{x}_0}^{\boldsymbol{x}_n} \boldsymbol{f}^{surf} dx \right] da \tag{2.49}$$

$$W_n^{body} = \int_\Omega \left[\int_{\boldsymbol{x}_0}^{\boldsymbol{x}_n} \boldsymbol{f}^{body} dx \right] dv \tag{2.50}$$

$$U_n^{kin} = \frac{1}{2} \int_\Omega \boldsymbol{v}_n^T \rho \boldsymbol{v}_n dv \tag{2.51}$$

$$U_n^{str} = \int_\Omega \left[\int^{\boldsymbol{\epsilon}_n} \boldsymbol{\sigma} d\boldsymbol{\epsilon} \right] dv \tag{2.52}$$

$$W_n^{dam} = \int_{\boldsymbol{x}_0}^{\boldsymbol{x}_n} c \boldsymbol{v} d\boldsymbol{x} \tag{2.53}$$

Within the context of a step-by-step finite element solution, and applying a trapezoidal integration rule, the following expressions can be derived,

$$W_n^{ext} = W_{n-1}^{ext} + \frac{1}{2} \sum_{i=1}^{N} \left\{ u_n^i - u_{n-1}^i \right\}^T \left\{ \left(\boldsymbol{f}_{n-1}^{ext} \right)^i + \left(\boldsymbol{f}_n^{ext} \right)^i \right\} \tag{2.54}$$

$$U_n^{kin} = \frac{1}{2} \boldsymbol{v}_n^T \boldsymbol{M} \boldsymbol{v}_n \tag{2.55}$$

which has to be determined based on midpoints velocities

$$U_n^{kin} = \frac{1}{2} \left(U_{n-\frac{1}{2}}^{kin} + U_{n+\frac{1}{2}}^{kin} \right) \tag{2.56}$$

and

$$U_n^{str} = U_{n-1}^{str} + \frac{1}{2} \sum_{i=1}^{N_{ip}} \left\{ \boldsymbol{\sigma}_{n-1}^i + \boldsymbol{\sigma}_n^i \right\}^T \Delta \boldsymbol{\epsilon}_n^i V^i \tag{2.57}$$

$$W_n^{dam} = W_{n-1}^{dam} + \frac{1}{2} \sum_{i=1}^{N} \left\{ \boldsymbol{u}_n^i - \boldsymbol{u}_{n-1}^i \right\}^T \boldsymbol{C} \left\{ \boldsymbol{v}_{n-1}^i + \boldsymbol{v}_n^i \right\} \tag{2.58}$$

where N and N_{ip} are the number of nodes and the number of integration points for the given body, respectively, $\boldsymbol{C} = c\boldsymbol{M}$ is the linear viscous damping matrix, and V^i is the volume associated to the integration point i.

Chapter 3

Discontinuum Contact Mechanics

3.1 Introduction

The pioneering work by Cundall and his colleagues, who completed the original work by Goodman in 1968 [27] on jointed rocks, marks the beginning of modelling of discontinuum media [28]. They developed an algorithm for modelling the behaviour of jointed rigid rocks, soon termed as *the Distinct Element Method.*

By advancing the capabilities of the finite element method, and increasing power of computing facilities, fully deformable blocks replaced the original rigid bodies, with the new *Discrete Element Method* terminology.

Nowadays, the discrete element method has reached to an ever increasing popularity for modelling all potential discontinuum media. Nevertheless, it is mainly used for two classes of problems:

- *Granular flow* : where a large number of simple elements (usually rigid) are interacting with each other and with the surrounding boundaries (rigid or deformable). Granular flow in silos and the slope stability analysis are the most attractable types of problems in this class.
- *Progressive fracture* : where a continuum is subjected to an extremely high condition such as explosive loading or high velocity impact, causing extensive cracking and possibly fragmentation. The behaviour of the model is continuously changing toward the discontinuity and the original geometry of the body is changing by the extension of cracking.

The essential point is that the finite element method is rooted in the concepts of continuum mechanics, thus not suited to general fracture propagation and fragmentation problems. The finite element method may only effectively deal with a single crack or a low fractured area without any fragmentation, whereas the discrete element method is specifically designed to solve problems that exhibit strong material and geometrical discontinuities.

Before dealing with the main issues, a quick review of historical developments and present industrial/scientific applications is provided.

3.1.1 Historical Development

As mentioned earlier, the original development of the discrete element method may be attributed to the work by Cundall in 1971. In the following, a brief review of the main historical developments of the method is provided:

- 1968 : Analysis of jointed rocks by Goodman [27].
- 1971 : Analysis of jointed rocks by Cundall [28].
- 1988 : Fully deformable discrete elements included (Ghaboussi [29]).
- 1990 : Beginning of large scale simulations.
- 1995 : Combined finite/discrete element method for fracture simulation of brittle media [3].
- 1995 : Coupling discrete elements with fluid or gas flow [30].
- 1996 : Parallel and object oriented computing [31, 32].
- 1996 : Modelling granular flow in silos [1].
- 1998 : Metal cutting using adaptivity techniques [33].
- 1998 : Impact analysis of anisotropic three dimensional composite shells [34].
- 1999 : Damage investigation and repair modelling of masonry structures/bridges.

It should be noted that for each case, earlier less sophisticated models can also be found in the literature and the mentioned years show the time of major advancements of the method.

3.2 Contact Detection

In this section, the contact detection procedures are briefly reviewed and their main advantage/disadvantage points are discussed [35]. Then, the alternating digital tree, as one of the fastest geometric intersection search algorithms, are explained in detail and its application to general contact detection problems will be reviewed by providing sample problems.

The problem of detecting the bodies that interact with each other, also known as the geometric intersection search, has become a serious computational task in multi-body analyses.

Assume there is a system of N interacting bodies; all may happen to come into contact with any other body. A naive contact detection method requires the checking for contact between each body and every other bodies within the system. Figure 3.1 shows how such a simple approach requires a checking link between each (target) body and the remaining (contactor) bodies.

The number of operations required to detect all contacts between N bodies will then be proportional to

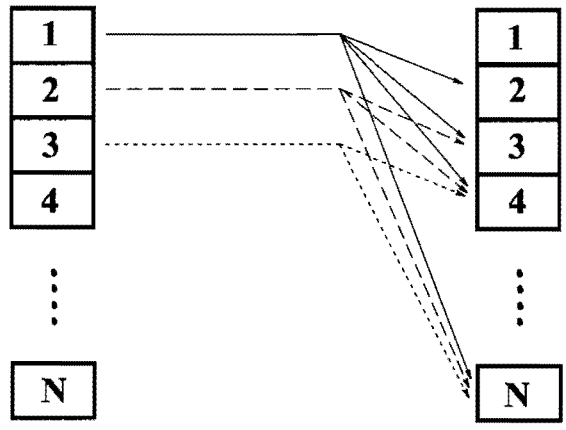

Figure 3.1: All to all check, the simplest contact detection procedure.

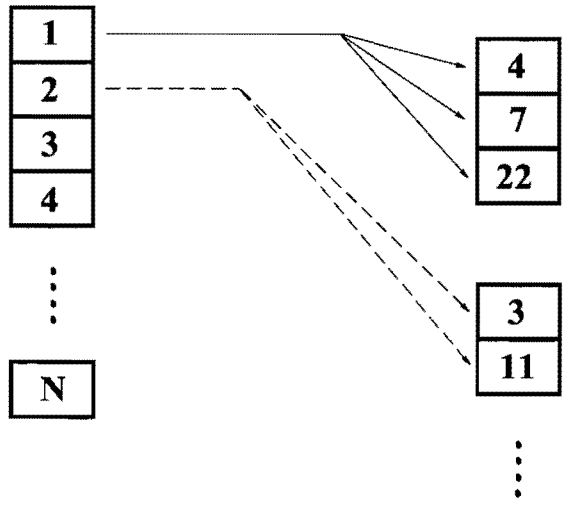

Figure 3.2: Short lists of contactors.

$$N\frac{N-1}{2} \tag{3.1}$$

In multibody analysis, however, the above method obviously becomes extremely expensive. Several other algorithms have been proposed to improve the detection procedure. In the best case, the computational efforts has been reduced to a factor of

$$N\log_2(N) \tag{3.2}$$

The existing detection methods have so far laid in between the two extremes.

The alternating digital tree (ADT) algorithm, which developed initially to solve the problem of mesh generation, reduces the number of operations required to determine the contacts between bodies by creation of short lists of potential contactors for each target body. Figure 3.2 shows a sample part of the created short list for a set of N contacting bodies. In this case, a direct checking is undertaken for the number of relevant bodies of a target, and the procedure is repeated for other target objects.

3.2.1 Contact Geometry

Depending on the type of modelling, two types of discrete elements may be defined:

1. Rigid bodies (Figure 3.3)

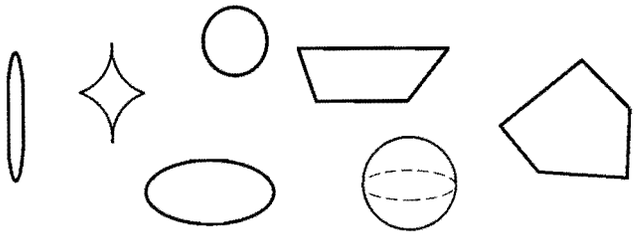

Figure 3.3: Simple rigid discrete elements.

2. Deformable finite elements (meshed polygons) (Figure 3.4)

The contact geometry is then either computed from the input definition of rigid bodies, e.g. a circular disc is defined by a centre point and radius, or automatically evaluated for deformable finite element bodies by evaluating all exterior edges/facets and grouping them for each discrete element, as depicted in Figure 3.5.

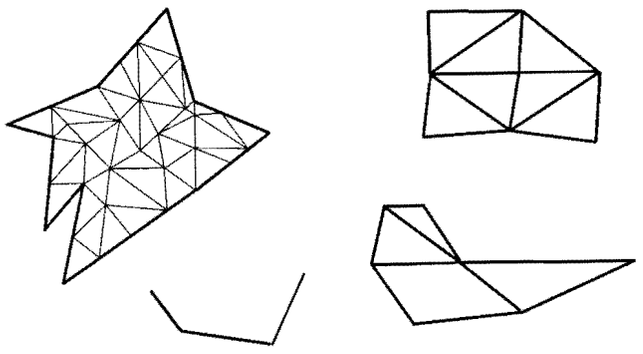

Figure 3.4: Deformable discrete elements (meshed polygons).

3.2.2 Global Search Algorithms

A general global search algorithm must be efficient in dealing with a large number of bodies, suitable for both rigid and deformable bodies, and efficient for both loose and tight packs of elements. A single approach might not achieve all the mentioned goals, and different approaches may be adopted for different applications.

3.2.3 Binary Tree Structures

A binary tree structure is a specific method of sorting data that allows new data to be easily added (inserted) or removed (deleted). Binary trees are one of the most important non sequential types of data structures. At each node, the information stored consists of data and two pointers known as the left and right links that point to further data. Each added link can either be equal to zero or equal to the position in memory where another node of the tree is placed.

Compared to a linear sequential array, the binary tree structure requires only two extra storage locations per item; left and right links, and provides a much greater degree of flexibility.

The first node in the tree is known as the root node. From one node of the tree it is possible to point at most two other nodes, while for each node (except the root), there is one and only one link pointing at it. A node without any pointer to other nodes is called a terminal node.

Figure 3.6 shows a typical binary tree structure with three levels of information and six nodes. The pointers on each node refer to the memory location for the left and right links, respectively. For example, pointer L_B refers to the memory location that holds the set of D data, i.e. left link to the B set.

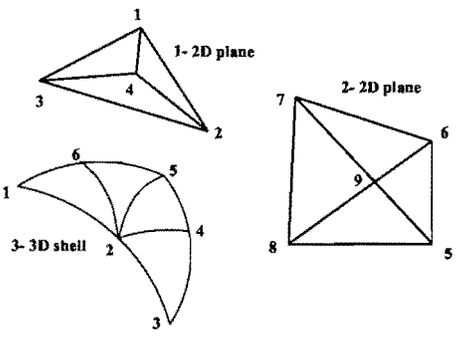

DE	Contact Geometry		
1	1	3	
	3	2	
	2	1	
2	5	6	
	6	7	
	7	8	
	8	5	
3	1	2	6
	2	3	4
	2	4	5
	5	6	2

Figure 3.5: Definition of contact geometries for discrete elements.

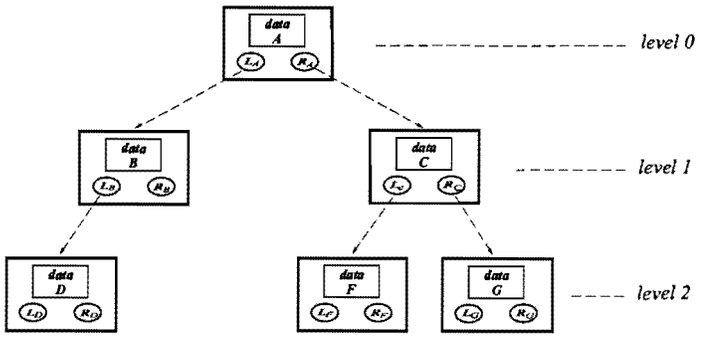

Figure 3.6: A simple binary tree data structure.

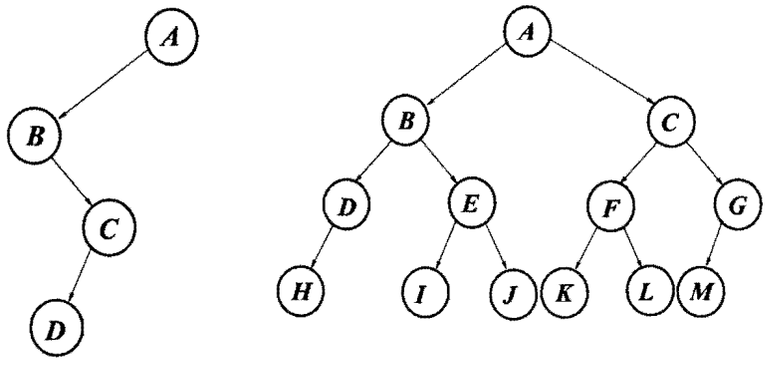

a) Degenerated tree b) Well balanced tree

Figure 3.7: Degenerated and well balanced binary trees.

Creation of a Binary Tree

The first step in creation of a binary tree structure is selecting a root node. Adding new data items to the binary tree depends on definition of a criterion for choosing between the left or the right branch for insertion. Every insertion then starts by checking this criterion at the root node and then traversing the tree until an empty place is found.

The criterion for insertion of data items and traversal of the binary tree is in fact a measure of relative spatial position of two nodes of the binary tree.

The order of object(body) insertion determines the final shape of the binary tree structure. The shape of the binary tree substantially influences the cost of the global contact searching as well as the cost of insertion of new data items. Poor performances are expected from highly degenerated binary trees (Figure 3.7a), as opposed to the very low insertion and search costs obtained from well balanced trees (Figure 3.7b).

An optimized ordering procedure for node insertion can be developed to consider the possibility of balancing a tree structure by adopting a new order of insertion. Such an optimized tree structure may be found extremely efficient if a binary tree for geometric intersection search has to be rebuilt and searched through relatively often.

3.3 Object Representation

In this chapter the main classes of object representation methods are discussed. It includes circular disks, ellipse shaped disks, and the general superquadric forms. Additionally, the meshed polygon systems, which frequently encountered in general finite element contact analyses are also among the

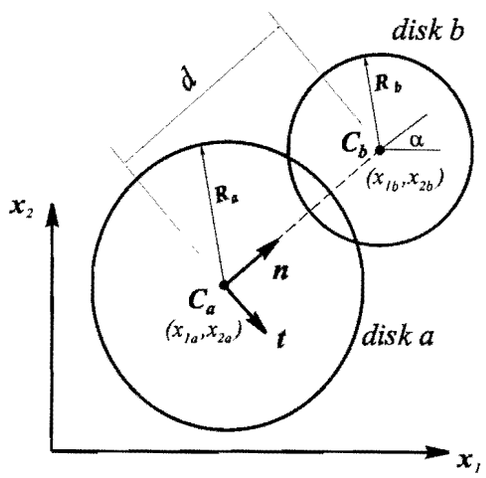

Figure 3.8: Geometry of two interacting disks.

object representation techniques. They usually provide specific problems within a contact detection or interaction procedure which have already been discussed and will not be addressed again.

3.3.1 Circular Disks

circular disks/spheres are probably the most frequently used type of element in modelling of granular flow by the discrete element method. They have been used as rigid body objects interacting each other in a granular flow simulation. Both penalty and continuum mechanics based methods have been used for contact interaction formulation.

From the object representation point of view, they consist the simplest forms for two and three dimensional modelling. Their geometric representation includes the coordinates of the centre and the magnitude of radius. The motion of particles can be readily calculated from the equations of rigid body dynamics.

Figure 3.8 shows the geometrical description of a system of two interacting 2D disks.

A relatively simple computational sequence for disk element analysis can be summarized according to the following:

For all contact pairs, follow the force-displacement law:

- Relative velocities $(i = 1, 2)$

$$\dot{X}_i = (\dot{x}_{ia} - \dot{x}_{ib}) - (\dot{\theta}_a R_a + \dot{\theta}_b R_b) t_i$$
$$\dot{n}_i = \dot{X}_i n_i \quad , \quad \dot{t}_i = \dot{X}_i t_i$$

- Relative displacements

  $\Delta n = \dot{n}\Delta t \quad , \quad \Delta t = \dot{t}\Delta t$

- Contact force increments

  $\Delta F_n = \alpha_n \Delta n \quad , \quad \Delta F_t = \alpha_t \Delta t$

- Total forces at time j

  $F_n^j = F_n^{j-1} + \Delta F_n \quad , \quad F_t^j = F_t^{j-1} + \Delta F_t$

- Check for slip

  $F_t = min(F_t, F_n tan\phi_\mu + c)$

For all particles, used the equations of motion

- Calculate moment

  $M_a = \sum F_a R_a \quad , \quad M_b = \sum F_b R_b$

- Assume constant force and moment from $t^{j-\frac{1}{2}}$ to $t^{j+\frac{1}{2}}$

- Acceleration

  $\ddot{x}_i^j = \frac{\sum F_i}{m} \quad , \quad \ddot{\theta}^j = \frac{\sum M}{I}$

- Velocity

  $\dot{x}_i^{j+\frac{1}{2}} = \dot{x}_i^{j-\frac{1}{2}} + \Delta t \ddot{x}_i^j$

  $\dot{\theta}^{j+\frac{1}{2}} = \dot{\theta}^{j-\frac{1}{2}} + \Delta t \ddot{\theta}^j$

- Assume constant velocities from t^j to t^{j+1}

- Displacements

  $x_i^{j+1} = x_i^j + \Delta t \dot{x}^{j+\frac{1}{2}}$

  $\theta^{j+1} = \theta^j + \Delta t \dot{\theta}^{j+\frac{1}{2}}$

At the end of sequence, the time is incremented and the whole procedure is repeated. A more sophisticated approach is presented here to clarify the main specifications of a disk based discrete element technique as described by Petrinic [1].

Normal Contact Force

Although the size of the overlap is small compared to the radii of the disks, only the contact zone is considered to be deformable. The contact force is assumed to be proportional to the overlap size of the two disks in contact and their relative velocity in the normal direction (model described in Figure 3.9),

$$F_n = P_n + C_n v_n^r \tag{3.3}$$

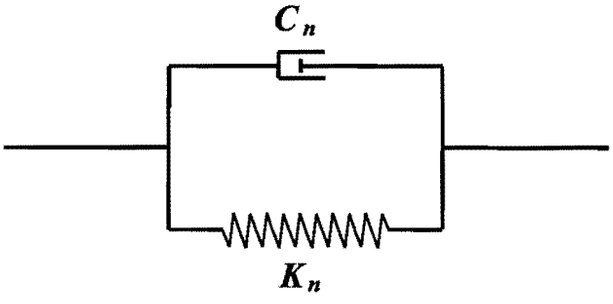

Figure 3.9: A model for normal contact force between two circular disks.

where $P_n = P_n(u)$ is the spring force , C_n is the viscous damping coefficient, v_n^r is the relative velocity in the direction normal to the contacting surfaces.

The spring force P_n is defined using the elasticity solution for two disks in contact,

$$P_n = \frac{\pi}{4} \frac{1 + \frac{K_4}{K_3}^2}{K_1 + K_2} \frac{R_1 + R_2}{R_1 R_2} b^2 \tag{3.4}$$

where R is the radius of disk, G is the shear modulus, ν is the poisson's ratio, b is half the width of the surface of contact (defined in Figure3.10) and,

$$\begin{aligned} K_1 &= \tfrac{1-\nu_1}{G_1} \\ K_2 &= \tfrac{1-\nu_2}{G_2} \\ K_3 &= \tfrac{2}{\pi}(K_1 + K_2) \\ K_4 &= \tfrac{1-2\nu_1}{G_1} - \tfrac{1-2\nu_2}{G_2} \end{aligned} \tag{3.5}$$

For small overlaps, the nonlinear spring behaves linearly which can be expressed as

$$P_n = K_n u_n \tag{3.6}$$

where K_n is the spring stiffness,

$$K_n = \left. \frac{dP_n}{du_n} \right|_{u_n=0} \tag{3.7}$$

The viscous damping coefficient is represented by a chosen percentage of the critical damping for a collision of two disks,

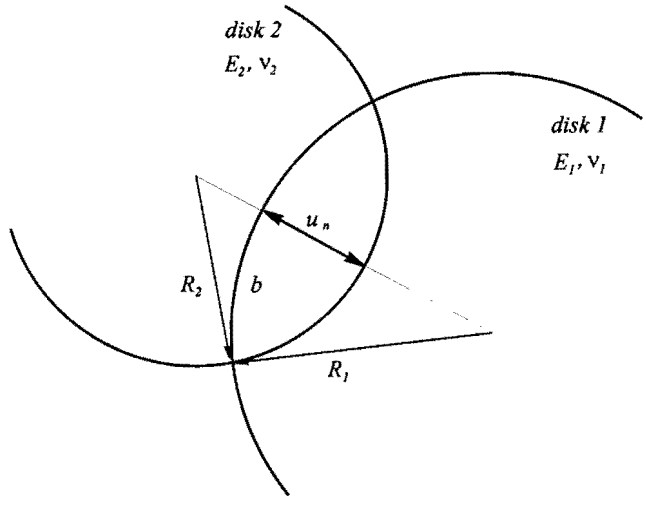

Figure 3.10: Normal contact between two circular disks.

$$C_n = \xi_n C_n^{cr} \tag{3.8}$$

$$C_n^{cr} = 2\sqrt{\frac{M_1 M_2}{M1 + M2} K_n} \tag{3.9}$$

where M_i is the mass of the disk i.

Tangential Contact Force

Geometrical idealization causes disks to be less resistant to rolling than the actual round shaped bodies they represent. Therefore, in order to model the formation of phenomena such as arching in granular flow using circular disks, an additional part of tangential component of contact force between disks has to be employed. Here, a so called rolling resistance is applied by means of a viscous damping force.

Sliding Friction

This part of the tangential component of contact force is represented by the model shown in Figure 3.11.

The actual expression for sliding friction is obtained following study of the sliding contact for locomotive driving wheels,

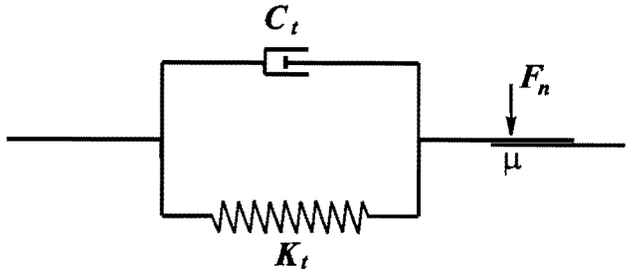

Figure 3.11: A model for sliding friction force between two circular disks.

$$F_t = P_t + C_t v_t^r \tag{3.10}$$

where $P_t = P_t(u_t)$ is the spring force defined as

$$P_t = \mu F_n \left[1 - \left(1 - \frac{u_t^r}{\frac{8}{\pi} F_n (K_1 + K_2) \frac{R_1 R_2}{R_1 + R_2}} \right)^2 \right] \tag{3.11}$$

where μ is the coefficient of friction, F_n is the normal component of the contact force, u_t^r is the relative tangential displacements of the contacting disks, C_t is the viscous damping coefficient and v_t^r is the relative tangential velocity.

The relative tangential displacement between the two disks is obtained from the solution of the global equations of motion,

$$u_t^r = u_{t-\Delta t}^r + v_t^r \Delta t_c \tag{3.12}$$

The relative tangential velocity is determined from the disks kinematics (Figure 3.12),

$$v_t^r = (\boldsymbol{v}_1 - \boldsymbol{v}_2) \cdot \boldsymbol{t} - (R_1 \omega_1 + R_2 \omega_2) \tag{3.13}$$

and the duration of contact is defined by:

$$\Delta t_c = min \left\{ \frac{u_n}{v_n^r}, \Delta t \right\} \tag{3.14}$$

where u_n is the size of normal overlap, Δt is the length of the time step during which the contact occurred and $\boldsymbol{v}$ is the disk velocity vector, while

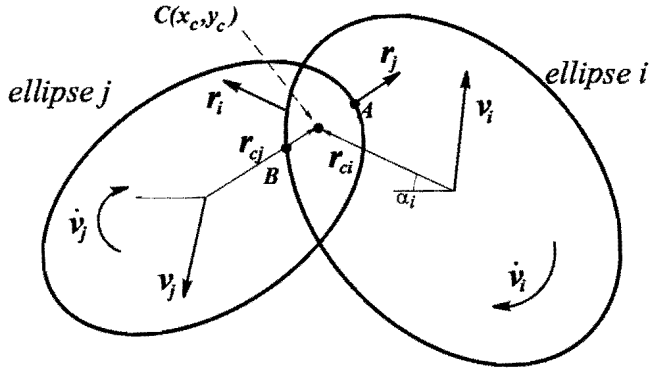

Figure 3.15: Contact between two ellipses.

$$\boldsymbol{v}_{ci} = (v_{xi} - \theta_i r_{ci} \sin\alpha_i)\boldsymbol{i} + (v_{yi} - \theta_i r_{ci} \cos\alpha_i)\boldsymbol{j} \tag{3.29}$$

The relative velocity of the contact between i and j is then

$$d\boldsymbol{v}_c = d\boldsymbol{v}_{cx}\boldsymbol{i} + d\boldsymbol{v}_{cy}\boldsymbol{j} \tag{3.30}$$

$$\begin{aligned} d\boldsymbol{v}_c = \quad & [(v_{xi} - \theta_i r_{ci} \sin\alpha_i) - (v_{xj} - \theta_j r_{cj} \sin\alpha_j)]\,\boldsymbol{i} + \\ & [(v_{yi} + \theta_i r_{ci} \sin\alpha_i) - (v_{yj} + \theta_j r_{cj} \sin\alpha_j)]\,\boldsymbol{j} \end{aligned} \tag{3.31}$$

where the terms with v are attributed to individual particle translation, and θ to particle rotation. This relative velocity may be resolved parallel and perpendicular to the contact normal to yield the incremental normal and tangential contact velocities:

$$\begin{aligned} d\boldsymbol{v}_{cn} &= dv_n\boldsymbol{n} = (d\boldsymbol{v}_c \cdot \boldsymbol{n})\boldsymbol{n} \\ &= (dv_{cx}n_1 + dv_{cy}n_2)\boldsymbol{n} \end{aligned} \tag{3.32}$$

$$\begin{aligned} d\boldsymbol{v}_{ct} &= dv_t\boldsymbol{t} = (d\boldsymbol{v}_c \cdot \boldsymbol{t})\boldsymbol{t} \\ &= (dv_{cx}t_1 + dv_{cy}t_2)\boldsymbol{t} \end{aligned} \tag{3.33}$$

noting that

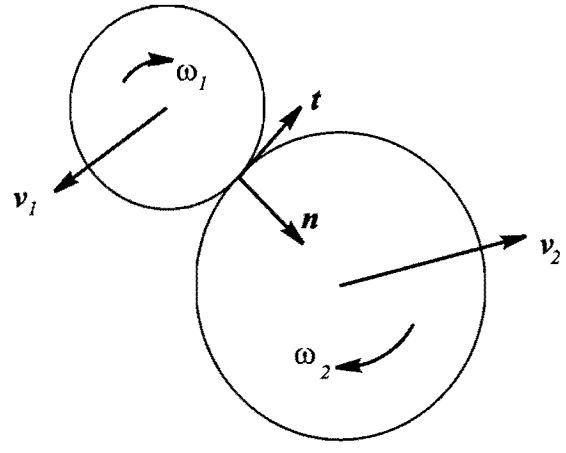

Figure 3.12: Kinematics of two contacting circular disks.

$$v_n^r = (\boldsymbol{v}_1 - \boldsymbol{v}_2) \cdot \boldsymbol{n} \tag{3.15}$$

is the relative normal velocity.

Figure 3.13 illustrates the relation between the relative tangential displacement and the frictional spring force.

The viscous damping coefficient C_t is represented by a chosen percentage of the critical damping

$$C_t = \xi_t C_t^{cr} \tag{3.16}$$

$$C_t^{cr} = 2\sqrt{\frac{M_1 M_2}{M_1 + M_2} K_t} \tag{3.17}$$

with K_t as the spring stiffness

$$K_t = \left.\frac{dP_t}{du_t}\right|_{u_t=0} \tag{3.18}$$

Rolling Friction

Consider the situation where the disk is set to roll on a rough horizontal plane (Figure 3.14),

The sliding friction cannot provide any resistance to the movement of the disk rolling on a rough surface since there is no relative tangential velocity at the contact point ($v_t^r = 0$). Therefore, an

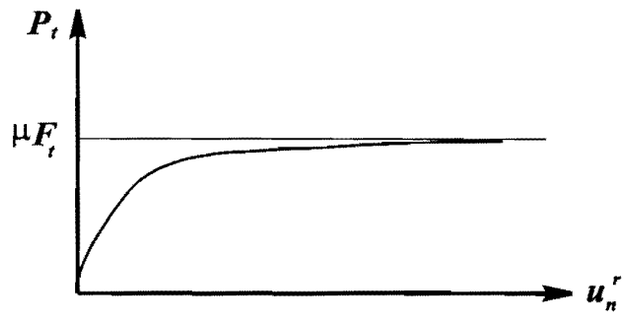

Figure 3.13: Relation between the relative tangential displacement and the frictional spring force.

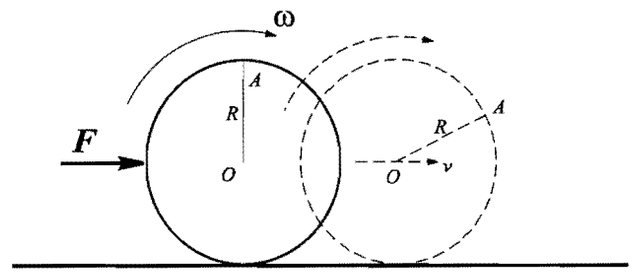

Figure 3.14: Rolling disk on a rough horizontal surface.

additional term for the tangential component of the contact force is also required; called the rolling friction,

$$F_r = C_r v_{tc}^r \tag{3.19}$$

where

$$C_r = \xi_r C_t^{cr} \tag{3.20}$$

is a chosen percentage of the critical damping (3.17), and

$$v_{tc}^r = (\boldsymbol{v}_1 - \boldsymbol{v}_2) \cdot \boldsymbol{t} \tag{3.21}$$

is the relative tangential velocity of the centroids of the disks in contact.

The rolling friction force should also satisfy the following condition

$$|F_t + F_r| \leq \mu F_n \tag{3.22}$$

Also, if the rolling friction obtained from (3.19) results in

$$|F_t + F_r| > F_n \tag{3.23}$$

it should be re-calculated in order to give priority to sliding

$$F_r = sign(v_{tc}^r)\,|\mu F_n - |F_t|| \tag{3.24}$$

Condition (3.22) is often satisfied automatically since the critical damping (3.17) depends on the sliding friction stiffness (3.20), which decreases when approaching the maximum allowed friction force μF_n (Figure 3.14). This is why the rolling part of the tangential component of the contact force is chosen to be applied in a form of damping. It ensures good co-operation of sliding and rolling friction.

Applying the force at the centroids of the disks also implies adding a resisting moment in the direction opposite to the direction of rolling as

$$M_r = -F_r R \tag{3.25}$$

3.3.2 Ellipse Shaped Particles

With more widespread use of disk and sphere based numerical codes, and the recent development of sphere based constitutive models for granular assemblages, it is particularly important to assess the degree to which these models are applicable for real non-spherical materials.

One common problem when using disk and sphere based discrete element modelling of soil is the low aggregate friction angle inherent in these systems, regardless of the angle of inter particle sliding friction, which is used.

Particle shape has the largest effect on mechanical behaviour, with reported increases in peak internal friction angle up to 10° for systems consisting of angular particles compared with round particles.

With the realization that disk based discrete element model has serious deficiencies when used for modelling real granular materials, it has recently become popular to use the ellipse as the basic particle shape. The ellipse shape has the advantage of having a unique and continuous outward normal and no singularities along its surface.

Solution for ellipse-ellipse contact detection requires solution of fourth degree algebraic equations, which can be done analytically rather than with iterative procedures. For these objects, normal contact forces acting eccentrically on a particle can generate applied moments which potentially inhibit particle rotation. As a result, this shape is well suited physically and numerically to modelling granular soils, powders and grains.

Contact Decomposition

Figure 3.15 indicates the nomenclature for two ellipses in contact. Points A and B, which can be used as a measure of the total normal overlap (penetration) between the two objects, are determined from the current ellipse-ellipse intersection algorithm.

To assess the relative importance of rolling and sliding mechanisms of deformation within the granular assemblage, the contact deformation is separated into portions due to individual particle rotation and particle translation.

For particle i, the vector from the centroid in the direction of the presumed point of contact is:

$$\boldsymbol{r}_{ci} = \boldsymbol{x}_c - \boldsymbol{x}_i \tag{3.26}$$

$$\boldsymbol{r}_{ci} = (r_{ci}\cos\alpha_i)\boldsymbol{i} + (r_{ci}\sin\alpha_i)\boldsymbol{j} \tag{3.27}$$

The velocity of the contact on particle i due to rotation and translation of i is:

$$\boldsymbol{v}_{ci} = \boldsymbol{v}_i + \theta_i \boldsymbol{k} \times \boldsymbol{r}_{ci} \tag{3.28}$$

$$\begin{aligned} t_1 &= n_2 \\ t_2 &= -n_1 \end{aligned} \tag{3.34}$$

where $\boldsymbol{n}$ is the unit outwards normal at the contact for ellipse i and $\boldsymbol{t}$ is the unit vector perpendicular to the normal, defined clockwise positive to particle i.

At a given instant, the individual terms in (3.32, 3.33) may be separated into the incremental net contact deformation, net normal contact deformation, or net tangential contact deformation due to particle translation or particle rotation.

The contribution of rotations of particle i and j to the net tangential contact deformation is:

$$d\boldsymbol{v}_c^{rt} = [(-\theta_i r_{ci} \sin\alpha_i) + (\theta_j r_{cj} \sin\alpha_j)]\,\boldsymbol{t}_2 - [(\theta_i r_{ci} \cos\alpha_i) - (-\theta_j r_{cj} \cos\alpha_j)]\,\boldsymbol{t}_1 \tag{3.35}$$

while the contribution to the net normal contact deformation is,

$$\begin{aligned} d\boldsymbol{v}_c^{rn} \quad = \quad & [(-\theta_i r_{ci} \sin\alpha_i) + (\theta_j r_{cj} \sin\alpha_j)]\,\boldsymbol{n}_1 + \\ & [(\theta_i r_{ci} \cos\alpha_i) - (-\theta_j r_{cj} \cos\alpha_j)]\,\boldsymbol{n}_2 \end{aligned} \tag{3.36}$$

The contribution of translation to the net tangential contact deformation is:

$$d\boldsymbol{v}_c^{tt} = [v_{xi} - v_{xj}]\,\boldsymbol{t}_2 - [v_{yi} - v_{yj}]\,\boldsymbol{t}_1 \tag{3.37}$$

$$d\boldsymbol{v}_c^{tn} = [v_{xi} - v_{xj}]\,\boldsymbol{n}_1 + [v_{yi} - v_{yj}]\,\boldsymbol{n}_2 \tag{3.38}$$

Numerical tests have shown that the particle rotation accounts for twice as much contact motion for round particles as does particle translations [36].

3.3.3 Superquadric Objects

Superquadrics (superquads) are a generalization of mathematical functions known as quadric surfaces. The extension comes about by raising the exponents of the variable terms to values other than 2. They are a family of parametric functions, introduced in mid 60's and later proposed for use in multibody dynamic analysis by Williams [37]. It is estimated that about 80 percent of all manufactured components can be represented by boolean combinations of the superquadric forms.

From the family of possible superquadric functions, the best known is the super ellipsoid [32]:

$$\mathcal{I}(x,y,z) = \left\{ \left|\frac{x-x_0}{a_1}\right|^{\frac{2}{\alpha}} + \left|\frac{y-y_0}{a_2}\right|^{\frac{2}{\alpha}} \right\}^{\frac{\alpha}{\beta}} + \left|\frac{z-z_0}{a_3}\right|^{\frac{2}{\beta}} \tag{3.39}$$

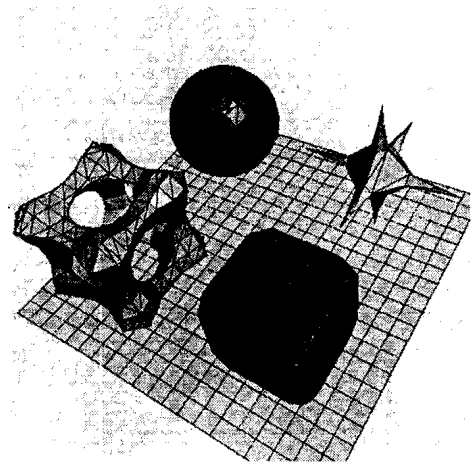

Figure 3.16: Superquadric elements [32].

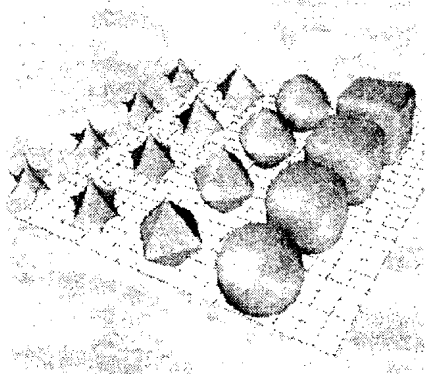

Figure 3.17: Superquadric elements [32].

where (x_0, y_0, z_0) is the origin of the function, (a_1, a_2, a_3) are the dimensions of the superquadric semi-major axes extents, and α and β are the roundness-squareness parameters of function in two perpendicular directions, respectively.

Figures 3.16 and 3.17 illustrate various objects that can be represented by a superquadric function.

Bibliography

[1] Petrinic, N., *Aspects of Discrete Element Modelling Involving Facet-to-Facet Contact Detection and Interaction.* Ph.D. thesis, Department of Civil Engineering, University of Wales Swansea, UK, 1996.

[2] Ortiz, M., Finite element analysis of impact damage and ballistic penetration. *Fourth US National Congress on Computational Mechanics, USNCCM IV*, ed. M. Shephard, pp. 10–13, 1997. San Francisco, USA.

[3] Munjiza, A., Owen, D. & Bicanic, N., A combined finite-discrete element method in transient dynamics of fracturing solids. *Engineering Computations*, **12**, pp. 145–174, 1995.

[4] Bicanic, N., Munjiza, A., Owen, D. & Petrinic, N., From continua to discontinua - a combined finite element / discrete element modelling in civil engineering. *Developments in Computational Techniques for Structural Engineering*, ed. B. Topping, Civil-Comp Press, pp. 1–13, 1995.

[5] Munjiza, A., *Discrete Elements in Transient Dynamics of Fractured Media.* Ph.D. thesis, Department of Civil Engineering, University of Wales Swansea, 1993.

[6] Lak, M., *Adaptive Shear Band Slope Stability Analysis.* Master's thesis, Department of Civil Engineering, University of Tehran, 2002.

[7] Stead, D., Eberhardt, E., Coggan, J. & Benko, B., Advanced numerical techniques in rock slope stability analysis - applications and limitations. *Landslides - causes, impacts and countermeasures*, pp. 615–624, 2001. Davos, Switzerland.

[8] Cramer, H., Findeiss, R., Steinl, G. & Wunderlich, W., An approach to the adaptive finite element analysis in associated and non-associated plasticity considering localization phenomena. *Computer Methods in Applied Mechanics and Engineering*, **176**, pp. 187–202, 1999.

[9] Petrinic, N., Owen, D., Munjiza, A. & Bicanic, N., Rolling resistance of disks in contact. *Extended Abstracts for the 3rd ACME UK Conference*, pp. 105–110, 1995. Oxford, UK.

[10] Williams, J. & Rege, N., Coherent structures in deforming granular materials. *International Journal of Mechanics of Cohesive-Frictional Materials*, 1996.

[11] Price, D., *Discrete element modelling of masonry walls.* Master's thesis, University of Wales Swansea, 1997.

[12] Yu, J., *A contact interaction framework for numerical simulation of multi-body problems and aspects of damage and fracture for brittle materials.* Ph.D. thesis, University of Wales Swansea, 1999.

[13] Klerck, P., *Finite element modelling of discrete fracture in quasi-brittle materials.* Ph.D. thesis, University of Wales Swansea, 2000.

[14] Marefat, M., Ghahremani-Gargari, E. & Naderi, R., Full scale test of a 60-year old mass-concrete arch bridge. *World Congress on Railway Research*, pp. 114–118, 2001. Koln, Germany.

[15] Ostadhossein, H., *Combined Finite/Discrete Element Modelling of Masonry Structures.* Master's thesis, Department of Civil Engineering, University of Tehran, 2001.

[16] Limited, R.S., Elfen helps save our historic structures. Newsletter 4, 2001.

[17] Hallquist, J., Goudreau, G. & Benson, D., Sliding interfaces with contact-impact in large-scale lagrangian computations. *Computer Methods in Applied Mechanics and Engineering*, **51**, 1985.

[18] Cundall, P. & Hart, R., Numerical modelling of discontinua. *1st US Conference on Discrete Element Methods*, eds. G. Mustoe, M. Henriksen & H. Huttelmaier, CSM Press, 1989.

[19] Peric, D. & Owen, D., Computational model for 3-d contact problems with friction based on the penalty method. *International Journal For Numerical Methods in Engineering*, **35**, pp. 1289–1309, 1992.

[20] Crook, A., Combined finite/discrete element method. Lecture Notes, Department of Civil Engineering, University of Wales Swansea, 1996.

[21] Schonauer, M., Rodic, T. & Owen, D., Numerical modelling of thermomechanical processes related to bulk forming operations. *Journal De Physique IV*, **3**, pp. 1199–1209, 1993.

[22] Munjiza, A., Bicanic, N., Owen, D. & Ren, Z., The central difference time integration scheme in contact-impact problems. *4th International Conference on Nonlinear Engineering Computations - NEC-91*, eds. N. Bicanic, P. Marovic, D. Owen, V. Jovic & A. Mihanovic, pp. 569–575, 1991.

[23] Zienkiewicz, O. & Taylor, R., *The Finite Element Method.* McGraw Hill, 4th edition, 1994.

[24] Hashimoto, K., Neto, E.S., Peric, D. & Owen, D., A study on dynamic frictional behaviour of coated steel sheets: experiments, formulation and finite element simulations. Technical report, University College of Swansea, 1993.

[25] Mohammadi, S., Owen, D. & Peric, D., Delamination analysis of composites by discrete element method. *Computational Plasticity, COMPLAS V*, eds. D. Owen, E. Onate & E. Hinton, pp. 1206–1213, 1997. Barcelona, Spain.

[26] Mohammadi, S., Owen, D. & Peric, D., Discontinuum approach for damage analysis of composites. *Computational Mechanics in UK - 5th ACME Conference*, ed. M. Crisfield, pp. 40–44, 1997. London, UK.

[27] Goodman, R., Taylor, R. & Brekke, T., A model for mechanics of jointed rock. *Journal of Solid Mechanics and Foundation, ASCE, SM3*, p. 94, 1968.

[28] Cundall, P., A computer model for simulating progressive, large scale movements in blocky rock system. *Proceedings of International Symposium on Rock Structures*, 1971. Nancy, France.

[29] Ghaboussi, J., Fully deformable discrete element analysis using a finite element approach. *Computers and Geotechnics*, **5**, pp. 175–195, 1988.

[30] Foster, N. & Metaxas, D., Visualization of dynamic fluid simulations: waves, splashing, vorticity, boundaries, buoyancy. *Engineering Computations*, **12**, pp. 109–124, 1995.

[31] Hustrulid, A. & Hall, B., Parallel implementation of the discrete element method. Technical report, Colorado School of Mines, 1996.

[32] O'Connor, R., *A Distributed Discrete Element Modelling Environment - Algorithms, Implementation and Applications*. Ph.D. thesis, Department of Civil and Environmental Engineering, MIT., 1996.

[33] Vaz-Jr., M., *Computational approaches to simulation of metal cutting process*. Ph.D. thesis, Deptartment of Civil Engineering, University of Wales Swansea, 1998.

[34] Mohammadi, S., *Combined Finite/Discrete Element Analysis of Impact Loading of Composite Shells*. Ph.D. thesis, Deptartment of Civil Engineering, University of Wales Swansea, 1998.

[35] Wensel, O., *Search algorithm for detecting geometric overlapping in a discrete element context*. Master's thesis, University of Wales Swansea, 1992.

[36] Ting, J., Meachum, L. & Rowell, J., Effect of particle shape on the strength and deformation mechanisms of ellipse-shaped granular assemblages. *Engineering Computations*, **12**, pp. 99–108, 1995.

[37] Williams, J., Contact analysis of large numbers of interacting bodies using discrete modal methods for simulating material failure on the microscopic scale. *Engineering Computations*, **5(3)**, pp. 150–161, 1988.